Impact of Climate Change on River Discharge Projected by Multimodel Ensemble

DAISUKE NOHARA

Meteorological Research Institute, Tsukuba, and CREST, Japan Science and Technology Agency, Kawaguchi, Japan

AKIO KITOH AND MASAHIRO HOSAKA

Meteorological Research Institute, Tsukuba, Japan

TAIKAN OKI

Institute of Industrial Science, University of Tokyo, Tokyo, Japan

(Manuscript received 26 April 2005, in final form 5 January 2006)

ABSTRACT

This study investigates the projections of river discharge for 24 major rivers in the world during the twenty-first century simulated by 19 coupled atmosphere–ocean general circulation models based on the Special Report on Emissions Scenarios A1B scenario. To reduce model bias and uncertainty, a weighted ensemble mean (WEM) is used for multimodel projections. Although it is difficult to reproduce the present river discharge in any single model, the WEM results produce more accurate reproduction for most rivers, except those affected by anthropogenic water usage. At the end of the twenty-first century, the annual mean precipitation, evaporation, and runoff increase in high latitudes of the Northern Hemisphere, southern to eastern Asia, and central Africa. In contrast, they decrease in the Mediterranean region, southern Africa, southern North America, and Central America. Although the geographical distribution of the changes in precipitation and runoff tends to coincide with that in the river discharge, it should be emphasized that the change in runoff at the upstream region affects the river flow in the downstream region. In high-latitude rivers (Amur, Lena, MacKenzie, Ob, Yenisei, and Yukon), the discharge increases, and the peak timing shifts earlier because of an earlier snowmelt caused by global warming. Discharge tends to decrease for the rivers in Europe to the Mediterranean region (Danube, Euphrates, and Rhine), and southern United Sates (Rio Grande).

1. Introduction

Projections of precipitation and river runoff associated with climate change are important sources of information for utilization of global water resources and prevention of floods and drought (Seckler et al. 1999; Vörösmarty et al. 2000; McCarthy et al. 2001; Milly et al. 2002; Oki et al. 2003; Arnell 2004). The development of coupled atmosphere–ocean general circulation models (AOGCMs) has enabled us to project future changes in precipitation and river runoff (Arnell 1999; Arora and Boer 2001; Manabe et al. 2004). Arnell (1999) has projected the global river discharge simulated by the Hadley Centre climate model and suggested that the annual runoff increases in high-latitude regions, equatorial Africa, and Southeast Asia, but it decreases in midlatitudes and most subtropical regions. However, Arora and Boer (2001) have shown that the annual river discharge decreases in equatorial Africa and Southeast Asia. Therefore, the projection of runoff is greatly dependent on AOGCM characteristics, which are still difficult to validate against appropriate observations.

In high latitudes of the Northern Hemisphere, the future freshwater discharge from major rivers is projected to increase, according to AOGCM simulations and statistical extrapolation using observations (Peterson et al. 2002; Wu et al. 2005; Arnell 2005). An increasing freshwater discharge into the Arctic Ocean presumably will affect the global climate system by slowing down the thermohaline circulation. From an analysis of observed river discharge data, Peterson et al. (2002) reported that the discharge of freshwater into

Corresponding author address: Dr. Akio Kitoh, Climate Research Department, Meteorological Research Institute, 1-1 Nagamine, Tsukuba, Ibaraki 305-0052, Japan.
E-mail: kitoh@mri-jma.go.jp

the Arctic Ocean increased by 7% from 1936 to 1999. Furthermore, Peterson et al. (2002) projected an increase in discharge between 18% and 70% by 2100 based on an extrapolation using increments of global surface air temperatures projected by the Intergovernmental Panel on Climate Change (IPCC) (Houghton et al. 2001) and on correlations between the observed discharge and the surface air temperature data. Arnell (2005) estimated a 31% (24%) increase in discharge into the Arctic Ocean by the 2080s under high (low) CO_2 emission scenarios using six AOGCM simulations.

Recently, various modeling groups have performed new simulations including the historical simulations [twentieth-century experiments (20C3M)] and future climate simulations (Meehl et al. 2005) based on the Special Report on Emissions Scenarios (SRES) (Nakicenovic and Swart 2000; Arnell et al. 2004). The SRES includes six marker scenarios (A1, A1B, A1FI, A2, B1, and B2) for projections of the world population, economy, and political structure for the next 100 yr. Simulated results based on the SRES scenarios are assessed by IPCC for projections of changes in the climate and their potential impact. The SRES A1B scenario, which represents a very rapid economic growth with increasing globalization into the future, is chosen for this study. The SRES A1B scenario projects a CO_2 concentration of 720 ppmv by the year 2100. The analysis method using multiple AOGCMs (called multimodel ensemble) is known to effectively improve the model projection by reducing characteristic biases and uncertainties of any individual model.

An analysis method using the multimodel ensemble has been developed for seasonal forecasting (Harrison et al. 1999; Krishnamurti et al. 1999; Palmer et al. 2000) and is applied also to climate change projections (Houghton et al. 2001; Giorgi and Mearns 2002; Min et al. 2004). The forecast skill of the multimodel ensemble mean is superior to that of each ensemble member (Fritsch et al. 2000). Giorgi and Mearns (2002) introduced a weighted multimodel ensemble mean (WEM) using information of the skill of the present climate simulations in order to increase the reliability of the projections. Min et al. (2004) investigated the future climate changes over East Asia using the multimodel ensemble of selected AOGCMs.

The purpose of this study is to project future river discharge using 19 AOGCM simulations based on the SRES A1B scenario. The river discharge is simulated in an offline mode by a river flow model that transports runoff water to the river outlet. To reduce model biases and uncertainties for the projection, the WEM is applied with new weights based on model performance. In addition, the change in future water circulation is discussed using the projections of precipitation, evaporation, and runoff.

The model implementation and data sources for this study are described in section 2. In section 3, the WEM is described and the present-day climate simulations are evaluated. The future projections of precipitation, evaporation, and runoff as well as simulated river discharges are shown in section 4. Finally, we present a summary and discussion in section 5.

2. Model implementation and data sources

a. Multimodel simulation

The dataset of experiments analyzed in this study includes 19 AOGCM simulations collected and archived at the Program for Climate Model Diagnosis and Intercomparison (PCMDI), as listed in Table 1. Variables analyzed include the monthly mean precipitation, evaporation, and runoff of the 20C3M and SRES A1B experiments. Evaporation is obtained by calculating the latent heat flux divided by the latent heat of vaporization by ignoring fusion and sublimation. The 20C3M experiment has been simulated by AOGCM with natural (e.g., volcanoes and solar) and anthropogenic (e.g., greenhouse gases, ozone, and aerosols) forcing in the twentieth century. The SRES A1B experiment has been calculated with projected external forcing by the SRES A1B scenario from the end of the 20C3M simulation to 2100.

All simulated results are converted to a common 2.5° by 2.5° grid by a bicubic spline interpolation scheme. The bicubic spline interpolation gives accurate values at the original grids and a smoothly varying field between them on a two-dimensional plane because the spline requires continuity to the second-order derivative at the grids.

b. River model

The river flow model used in this study is Global River flow model using Total Runoff Integrating Pathways (TRIP) (GRiveT) developed at the Meteorological Research Institute. TRIP is a global river channel network in a 1.0° by 1.0° grid developed by Oki and Sud (1998). The transport equation of the GRiveT in river channels is a simple flux form written as

$$\frac{dM}{dt} = R + \sum F_{\text{up}} - F_{\text{down}}, \tag{1}$$

where M is the water mass in the river channel of the grid, R is the input of the monthly runoff water simulated by each AOGCM, F_{up} is the summation of the water flux from the upstream grids, and F_{down} is the

TABLE 1. List of AOGCM simulations based on the IPCC SRES A1B and 20C3M.

Model name	Originating group	Resolution
CCSM3	National Center for Atmospheric Research, United States	T85L26
CGCM3.1(T47)	Canadian Centre for Climate Modelling and Analysis, Canada	T47L31
CNRM-CM3	Météo-France/Centre National de Recherches Météorologiques, France	T42L45
CSIRO-Mk3.0	CSIRO Atmospheric Research, Australia	T63L18
ECHAM5/MPI-OM	Max Planck Institute for Meteorology, Germany	T63L31
ECHO-G	Meteorological Institute of the University of Bonn, Meteorological Research Institute of KMA, and Model and Data group, Germany/Korea	T30L19
FGOALS-g1.0	LASG/Institute of Atmospheric Physics, China	T42L26
GFDL-CM2.1	Department of Commerce/NOAA/Geophysical Fluid Dynamics Laboratory, United States	M45L24
GISS-AOM	NASA Goddard Institute for Space Studies, United States	4.0×3.0L12
GISS-EH	NASA Goddard Institute for Space Studies, United States	5.0×4.0L20
GISS-ER	NASA Goddard Institute for Space Studies, United States	5.0×4.0L20
INM-CM3.0	Institute for Numerical Mathematics, Russia	5.0×4.0L21
IPSL-CM4	Institut Pierre Simon Laplace, France	2.5×3.75L19
MIROC3.2(hires)	Center for Climate System Research (University of Tokyo), National Institute for Environmental Studies, and Frontier Research Center for Global Change (JAMSTEC), Japan	T106L56
MIROC3.2(medres)	Center for Climate System Research (University of Tokyo), National Institute for Environmental Studies, and Frontier Research Center for Global Change (JAMSTEC), Japan	T42L20
MRI-CGCM2.3.2	Meteorological Research Institute, Japan	T42L30
PCM	National Center for Atmospheric Research, United States	T42L18
UKMO-HadCM3	Hadley Centre for Climate Prediction and Research/Met Office, United Kingdom	2.5×3.75L19
UKMO-HadGEM1	Hadley Centre for Climate Prediction and Research/Met Office, United Kingdom	1.25×1.875L38

water flux to the downstream grid. The flux F is parameterized as

$$F = \frac{u}{d} M, \tag{2}$$

where u is the effective flow velocity of the river routing and d is the distance between grid boxes. The effective flow velocity is set at 0.40 m s^{-1} for all rivers following studies that use flow velocities ranging from 0.3 to 0.5 m s^{-1} (Oki et al. 1999), although it is known that flow velocities are not constant and can vary widely from 0.15 to 2.1 m s^{-1} (Arora and Boer 1999). In the process of simulation, GRiveT distributes the runoff water on the model grids to TRIP grids with a weight that is estimated by the ratio of the overlaid area on both grids. After that, GRiveT transports the runoff water to the river outlet along the river channel by TRIP. GRiveT excludes any human usage of the river water, such as irrigation and dams, and any natural effect, such as evaporation from the channel and loss of river water through infiltration in the riverbed.

c. River discharge data

To validate the simulated river discharge, observed monthly river discharge records are obtained from the Global Runoff Data Centre (GRDC; in Koblenz, Germany). The 24 river basins based on TRIP and locations of the discharge observation stations selected for this study are drawn in Fig. 1. The selected rivers are distributed in all continents and in various climatic zones, including tropical (Amazon and Congo), arid (Amu Darya, Euphrates, Huang He, Murray, Nile, Rio Grande, and Syr Darya), midlatitude rainy (Columbia, Danube, Mississippi, Parana, Rhine, and Volga), Asian monsoon (Changjiang, Ganges, and Mekong), and high latitudes (Amur, Lena, MacKenzie, Ob, Yenisei, and Yukon). The observed river discharges do not necessarily represent natural discharges, because river discharges are affected by evaporation from the river surface and an artificial control of the river flow (e.g., irrigation, diversions, and dams).

3. Model evaluation

We first evaluate the present climate simulations of 19 AOGCMs in terms of reproducibility of precipitation by comparing with the Global Precipitation Climatology Project (GPCP) dataset (Adler et al. 2003). The model resolutions and parameterizations differ from one another. Therefore, each AOGCM has a different performance in reproducing the spatial and temporal distribution in precipitation, evaporation, and runoff. It is assumed here that a skillfully designed model for

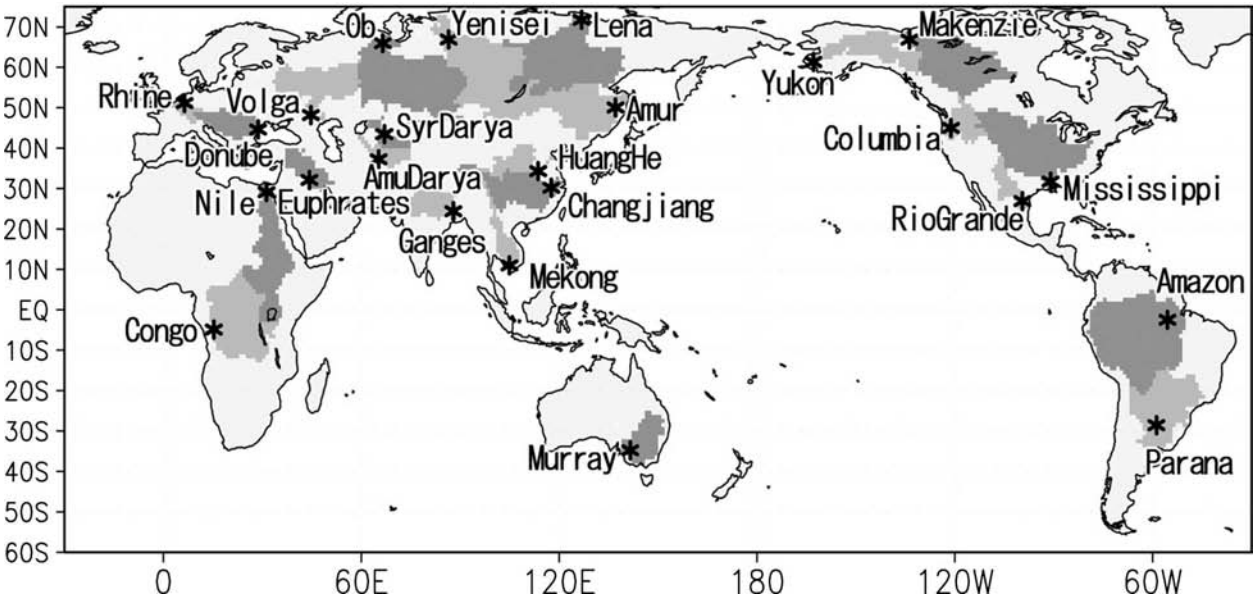

FIG. 1. The 24 major river basins selected. The asterisks indicate the location of the discharge observations.

reproducing precipitation could produce more reliable estimates of the amount and distribution in runoff and evaporation, because simulated precipitation is an outcome as a consequence of the atmosphere–ocean general circulation and land surface scheme.

To evaluate the model performance, we use the global averaged annual mean precipitation (MEAN), root-mean-square (RMS) difference, and pattern correlation (R). RMS and R are defined as

$$\mathrm{RMS} = \sqrt{\frac{\sum_{i=1}^{n} w_i (P_{s,i} - P_{o,i})^2}{\sum_{i=1}^{n} w_i}}, \tag{3}$$

$$R = \frac{\sum_{i=1}^{n} w_i (P_{s,i} - \overline{P}_s)(P_{o,i} - \overline{P}_o)}{\sqrt{\sum_{i=1}^{n} w_i (P_{s,i} - \overline{P}_s)^2} \sqrt{\sum_{i=1}^{n} w_i (P_{o,i} - \overline{P}_o)^2}}, \tag{4}$$

where $P_{s,i}$ and $P_{o,i}$ are the simulated and observed precipitation in grid point i, w_i is the area weight, and the overbar is the global mean. Notice that the global mean is defined as the regional mean from 60°S to 75°N, since no river or observation station of discharge exists in the Arctic or Antarctic.

Table 2 presents the MEAN, RMS, and R for each AOGCM averaged from 1981 to 2000 based on 20C3M

TABLE 2. Annual mean precipitation (MEAN, mm day^{-1}), root-mean-square (RMS) difference, and pattern correlation (R) for the individual model relative to GPCP.

Models	MEAN	RMS	R	Models	MEAN	RMS	R
CCSM3	2.94	1.42	0.749	GISS-ER	3.10	1.73	0.673
CGCM3.1(T47)	2.89	1.32	0.771	INM-CM3.0	2.98	1.90	0.605
CNRM-CM3	3.45	1.62	0.697	IPSL-CM4	2.75	1.43	0.762
CSIRO-Mk3.0	2.65	1.27	0.761	MIROC3.2(hires)	3.10	1.30	0.802
ECHAM5/MPI-OM	3.07	1.56	0.747	MIROC3.2(medres)	2.83	1.16	0.815
ECHO-G	2.90	1.16	0.817	MRI-CGCM2.3.2	2.69	1.10	0.851
FGOALS-g1.0	3.08	1.26	0.765	PCM	3.25	1.99	0.552
GFDL-CM2.1	3.03	1.32	0.797	UKMO-HadCM3	3.05	1.63	0.792
GISS-AOM	3.00	1.53	0.690	UKMO-HadGEM1	3.19	1.97	0.655
GISS-EH	3.13	1.78	0.622				
GPCP	2.74						

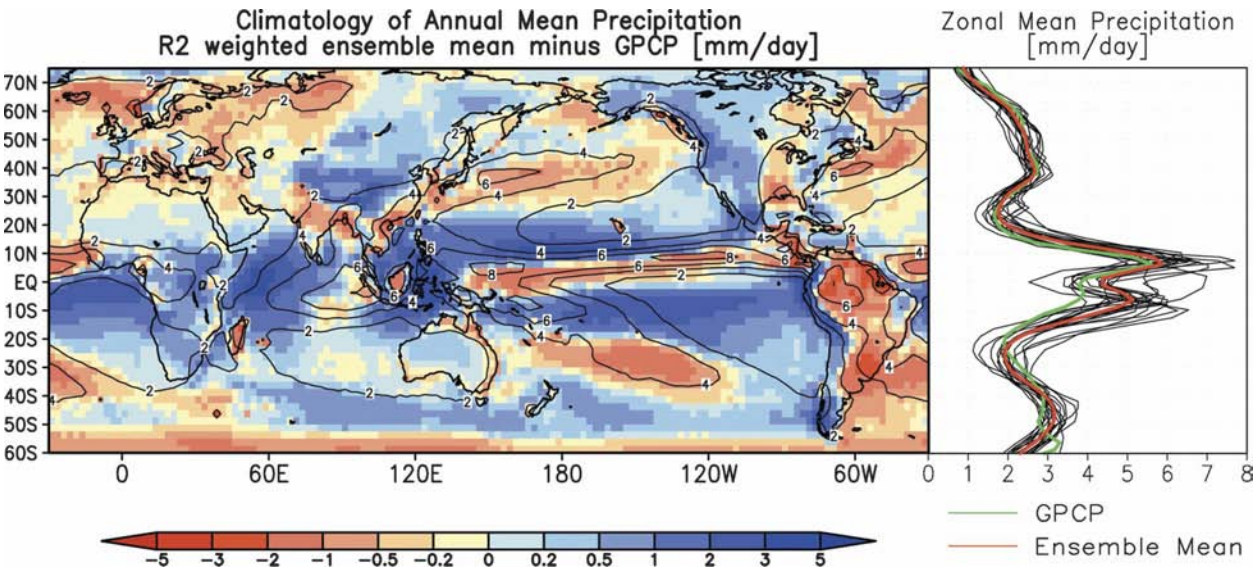

FIG. 2. Climatology of annual mean precipitation (mm day^{-1}). (left) The contour shows the observed precipitation by the GPCP, and the color shading shows the difference between WEM and GPCP. (right) The zonal mean precipitation is shown for the individual model (thin curves), WEM (solid red curve), and the observation (solid black curve).

relative to the GPCP averaged from 1979 to 2003. Most models have positive biases in MEAN, indicating that the AOGCMs tend to overestimate the global mean precipitation. Evaluation by RMS and R indicates that ECHO-G, MIROC3.2 (medres), and MRI-CGCM2.3.2 represent more quantitative coincidence of climatological precipitation than the other models.

The performance of the multimodel ensemble mean is also calculated (Table 3). The weighted ensemble mean is defined as the average of all models, weighted with a reciprocal number of RMS, R, and R^2. It is shown that the performance of all the weighted ensemble means is superior to that of the normal ensemble mean. In particular, the R^2 weighted ensemble mean results in the most skillful performance. Hereafter, the weighted multimodel ensemble mean using the determined coefficient R^2 is indicated as the WEM.

The difference of the annual mean precipitation between WEM and GPCP is plotted in Fig. 2. WEM overestimates the precipitation in central Africa, western North and South America, and eastern Eurasia. On the other hand, WEM underestimates the precipitation in eastern South America and Europe to western Eurasia. The global distribution and the zonal mean precipitation suggest that most models tend to produce a double intertropical convergence zone (ITCZ). The amount of the zonal mean precipitation simulated by an individual AOGCM significantly differs from the observations, although it is skillfully simulated in WEM, except in the tropical belt from the equator to 20°S.

4. Results

a. Future climate change

For the AOGCM experiments with the SRES A1B scenario, the WEM of the global (land) averaged surface air temperature at the end of the twenty-first century increases by +2.7 (+3.7) K relative to the present value (defined as the average from 1981 to 2000) (not shown). The land warms faster than the ocean, and greater relative warming occurs in high latitudes. Changes in surface air temperature directly interact with changes in precipitation. Figure 3 illustrates the WEM of the change in annual mean precipitation of the future (defined as the average from 2081 to 2100) against that of the present. Precipitation over land increases in high latitudes of the Northern Hemisphere, southern to eastern Asia, and central Africa. In contrast, it decreases in the Mediterranean region, southern Africa, and southern United States. Although the zonal mean precipitation coincides with this result, intermodel variability is large in the low- to midlatitude

TABLE 3. Performances of multimodel ensemble mean.

	RMS	R
Normal ensemble mean	1.02	0.851
Inverse RMS weighted ensemble mean	0.99	0.859
R weighted ensemble mean	1.00	0.857
R^2 weighted ensemble mean	0.98	0.862

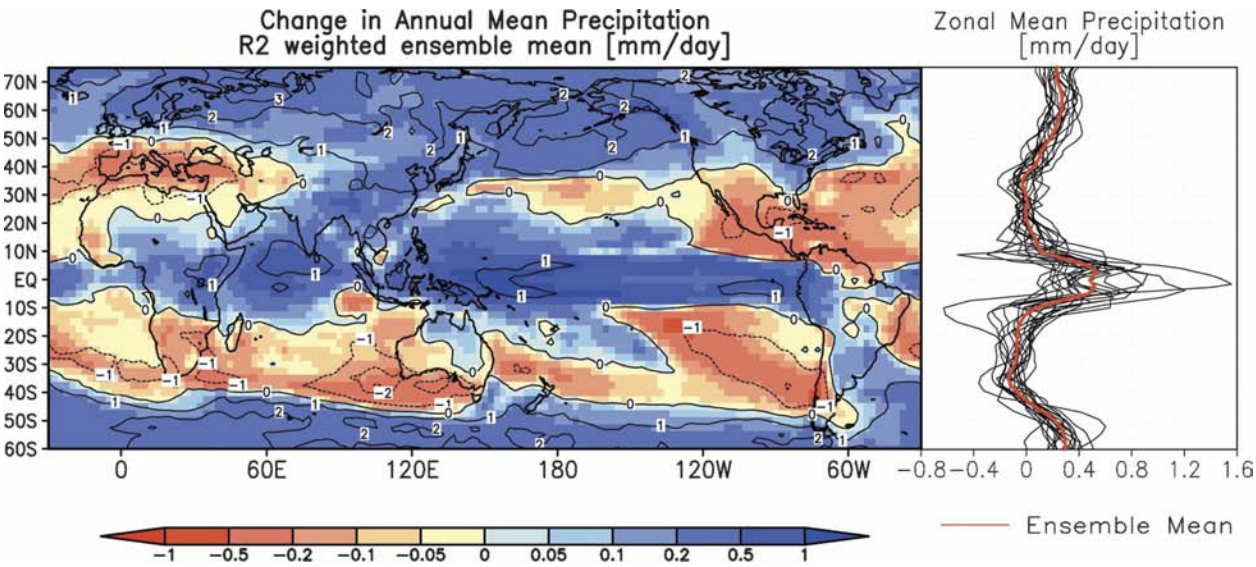

FIG. 3. Change in the annual mean precipitation (mm day^{-1}). (left) The color shading shows the WEM of the change in annual mean precipitation of the future against the present. The contour shows the normalized precipitation change. (right) The changes in the zonal mean precipitation of the individual model (thin curves) and the WEM (solid red curve) are shown.

areas. The normalized precipitation change is defined as the WEM of the precipitation change divided by the standard deviation of the changes in precipitation among the 19 models (Houghton et al. 2001). When the absolute value of the normalized precipitation change exceeds 1, the WEM of the precipitation change exceeds the intermodel variability of the precipitation change, and thus the result is considered to be significant. Based on the WEM, the future precipitation increases in eastern Asia (+0.2 mm day^{-1}), in high latitudes (+0.1 mm day^{-1}), and in parts of central Africa (+0.5 mm day^{-1}). In contrast, it decreases in the Mediterranean region (−0.2 mm day^{-1}), in parts of southern Africa (−0.2 mm day^{-1}), and in Central America (−0.5 mm day^{-1}).

The smoothed time series of the global mean and land mean annual precipitation change relative to the present for the WEM and the individual models are calculated with a 10-yr running mean (Fig. 4). The precipitation changes of most models and the WEM exhibit increasing trends over the globe and over the land. The intermodel variability of the land mean precipitation change is larger than that of the global mean precipitation change. The global mean and land mean precipitation of the WEM for the 2090s increase by 4.1% (0.122 mm day^{-1}) and 5.0% (0.114 mm day^{-1}), respectively.

The simulated surface water supplied by precipitation is used for evaporation and runoff in the individual land surface models. Generally, increasing temperature results in increasing potential evaporation because the

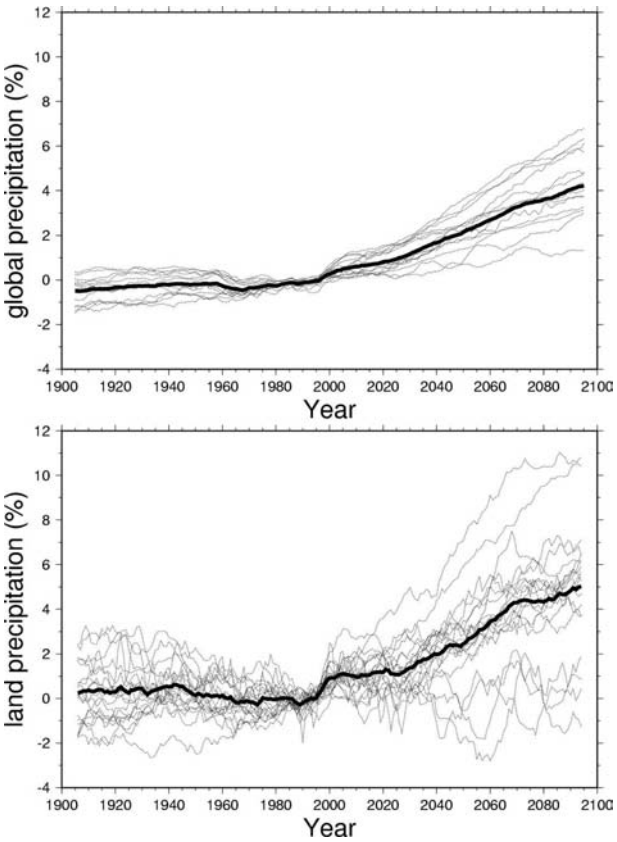

FIG. 4. Smoothed time series of the (top) global mean and (bottom) land mean precipitation change relative to the present for the WEM (solid thick curve) and the individual model (dotted curves) with a 10-yr running mean.

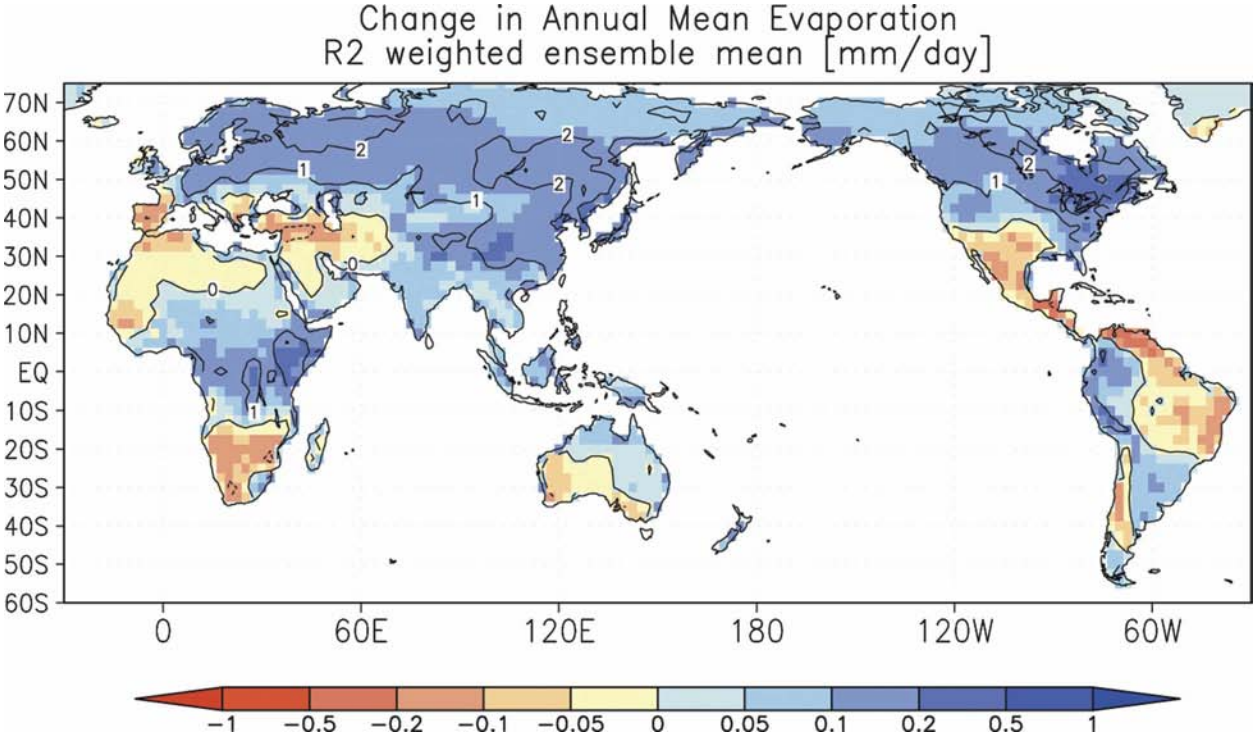

FIG. 5. Change in the annual mean evaporation (mm day^{-1}). The color shading shows the change in the WEM of the evaporation for the future against the present. The contour shows the normalized evaporation change.

water-holding capacity of the air increases. Figures 5 and 6 illustrate the future changes in the annual mean evaporation and runoff against that of the present. The evaporation and runoff increase in high latitudes, southern to eastern Asia, and central Africa, but decrease in the Mediterranean region, southern Africa, southern North America, and Central America. The amount of increased evaporation in high latitudes from 45° to 65°N is larger than that of increased runoff. On the other hand, the amount of increased runoff in southern to eastern Asia, the Amazon, and the Arctic tundra is larger than that of increased evaporation. The area extent with decreased runoff from the Mediterranean to central Eurasia and southern North America is larger than that with decreased precipitation and evaporation. It is noted that the area extent of highly reliable runoff change, which is represented by the normalized runoff change, is smaller than that of the precipitation and evaporation change. It implies that projecting the runoff change is more difficult than projecting the precipitation and evaporation changes, because the simulated runoff is obtained, by a first-order approximation, as a difference between precipitation and evaporation, and also includes uncertainty in the land surface scheme.

The smoothed (10-yr running mean) time series of the global mean runoff change relative to the present for the WEM and the individual models are plotted in Fig. 7. The runoff of most models and the WEM exhibit an increasing trend, but the intermodel variability of the runoff change is larger than that of the precipitation change. The global mean of the runoff change in the WEM increases by 8.9% (0.067 mm day^{-1}) in the 2090s, which is also larger than that of the precipitation change.

b. *Projection of river discharge*

GRiveT calculates river flow using the runoff obtained by each AOGCM. Figure 8 illustrates the simulated annual mean river flow for the present by the WEM and river flow change in the future relative to the present. The river flow increases in high latitudes, southern to eastern Asia, and central Africa. In contrast, it decreases in the Mediterranean region, southern Africa, southern North America, and Central America. Although the spatial distribution of the change of the river flow is similar to that of runoff, it should be emphasized that the change of runoff in the upstream region affects the river flow in the downstream region. For example, the runoff at the river outlet of the Euphrates (30°N, 50°E) increases in the future although the river flow decreases more than 20%.

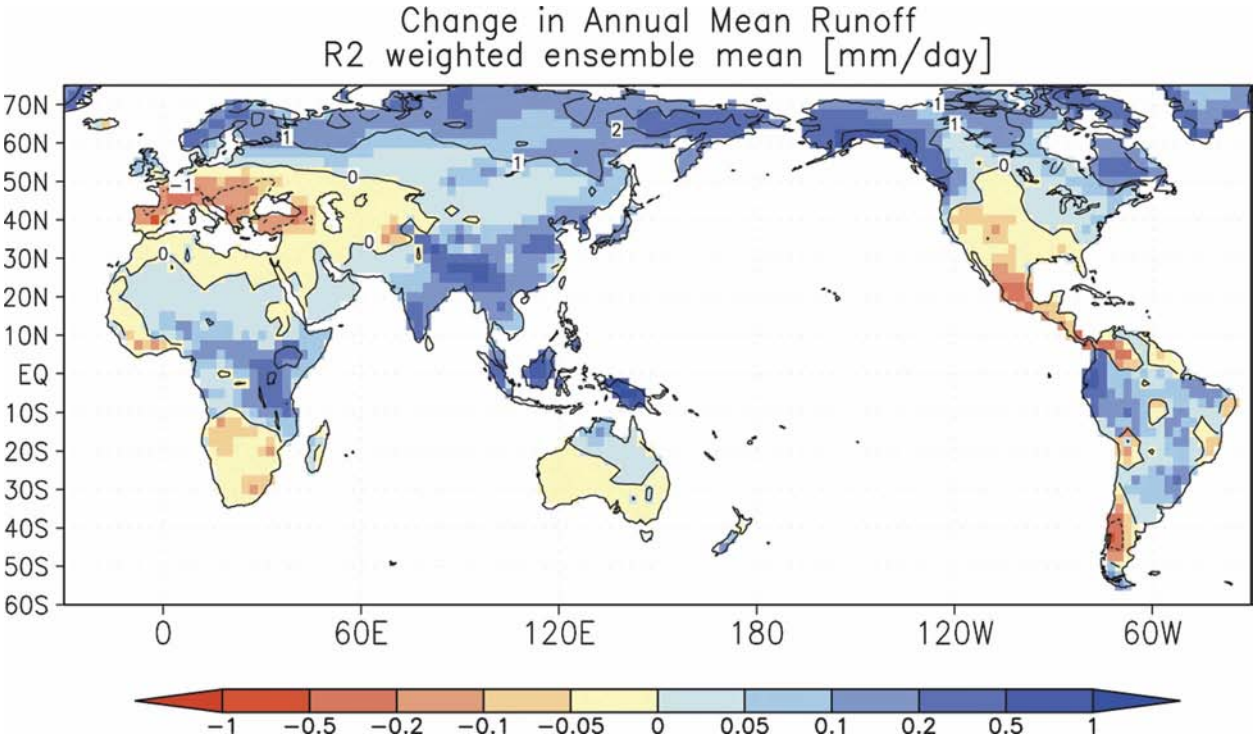

FIG. 6. As in Fig. 5, but for runoff.

On the other hand, at the Nile (30°N, 30°E), the runoff decreases even though the river flow increases.

Figure 9 illustrates the monthly hydrographs and discharge changes for the 24 rivers. Although the reproduced present discharges of the individual models spread widely around the observation, the WEM of discharges provides a more accurate reproduction. Table 4 lists the annual mean discharge of the observation, present simulation, and future projection. RRMS is defined as the relative root-mean-square error between the simulated present discharge and observation as follows:

$$\mathrm{RRMS} = \frac{\sqrt{\frac{1}{12}\sum_{m}(D_{p,m} - D_{o,m})^2}}{\overline{D}_o} \times 100, \qquad (5)$$

where $D_{p,m}$ and $D_{o,m}$ are the simulated present discharge and the observation in month m, and the overbar means the annual mean. The amount of RRMS for the reproducibility of the present discharge by the WEM is similar to the results by Nijssen et al. (2001), estimated by the macroscale hydrological model using reanalyzed meteorological forcing (e.g., precipitation, surface temperature, and radiation) based on station observations. The change with an asterisk in Table 4 indicates obvious increments or decrements of the future discharge estimated by the normalized discharge change; only two rivers (Danube and Lena) fall into this category.

In tropical rivers, the WEM of the discharge is roughly one-half (twice) of that from observations on the Amazon (Congo). Nevertheless, the seasonal cycle of the discharge from the Amazon behaves in the same way as the observed seasonal cycle. The annual mean discharge from the Amazon and the Congo for the future increases slightly (+5.4%, and +4.4%). From

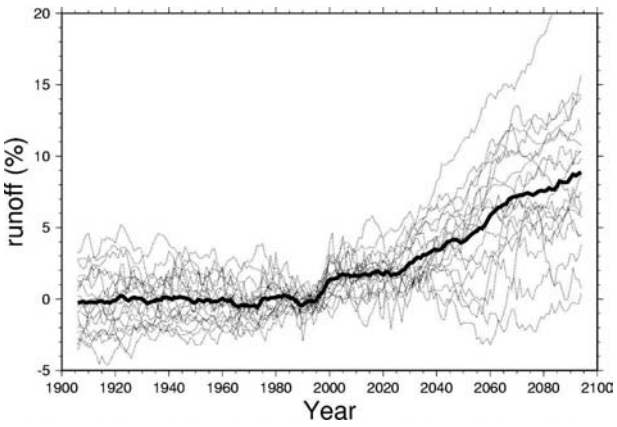

FIG. 7. Smoothed time series of the global mean runoff change relative to the present for the WEM (solid curve) and the individual model (dotted curves) with a 10-yr running mean.

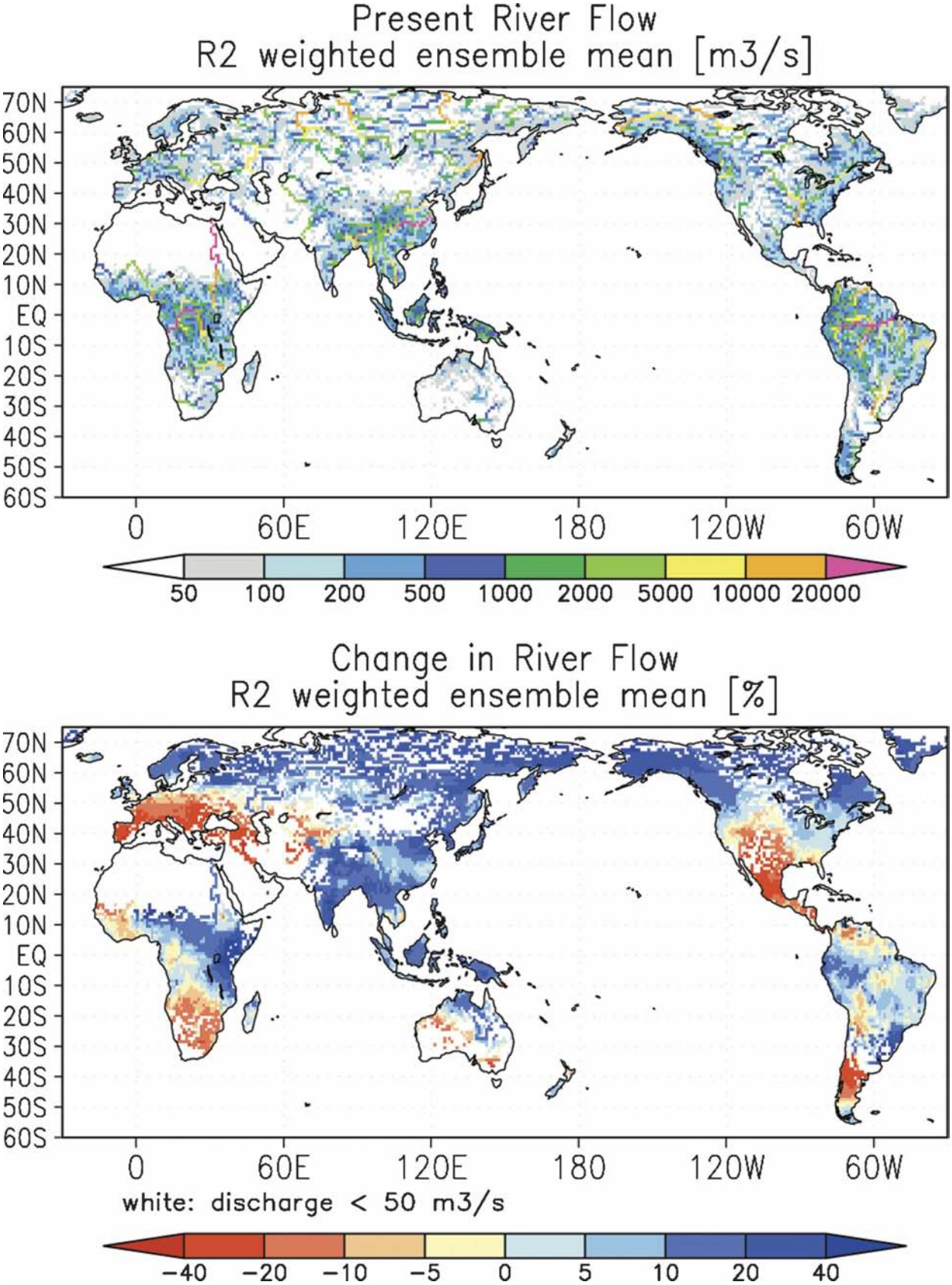

FIG. 8. (top) Simulated annual mean driver flow for the present by the WEM ($m^3 s^{-1}$); (bottom) river flow change in the future relative to the present (%).

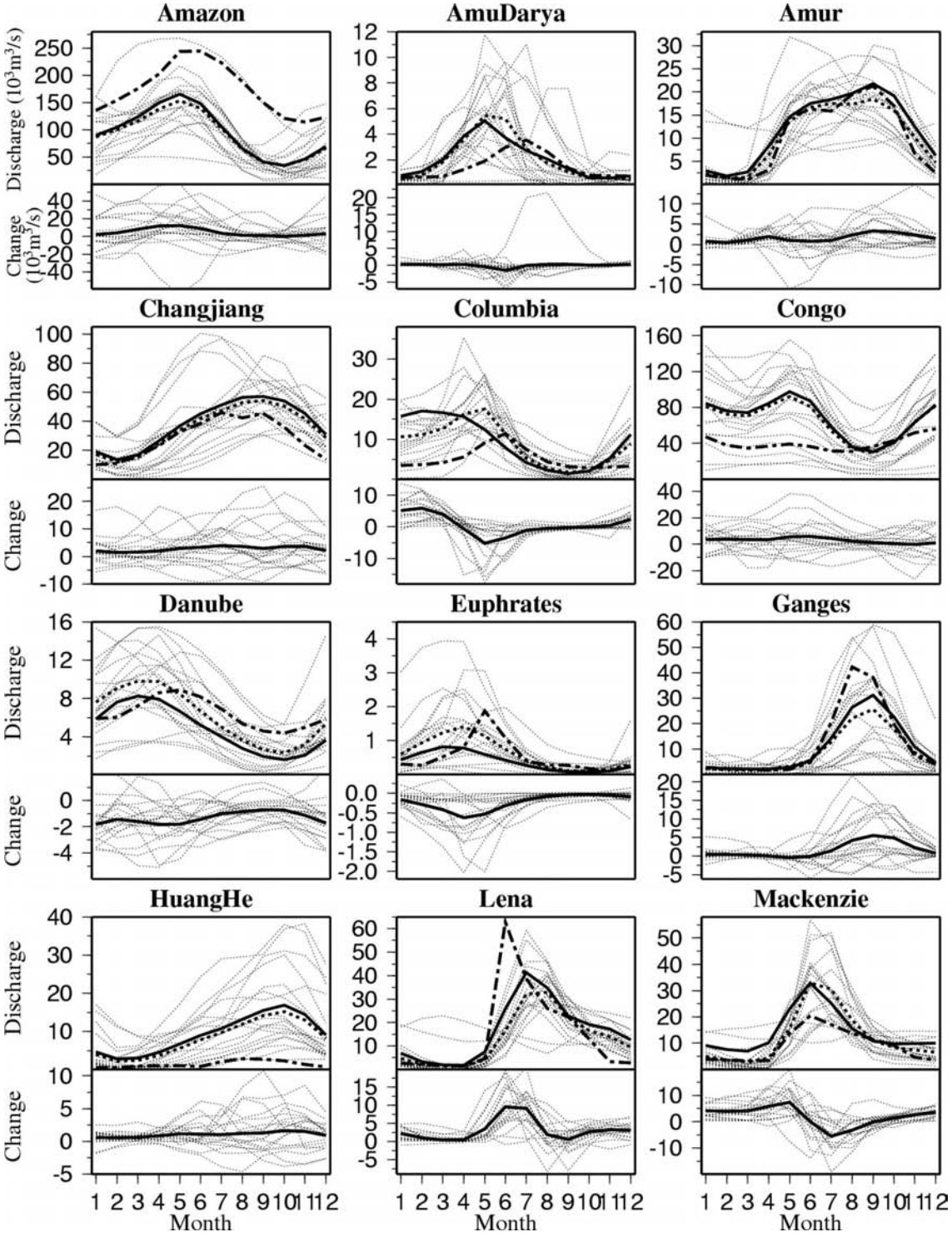

FIG. 9. (left) Monthly hydrographs and (right) discharge change for the 24 rivers (10^3 m^3 s^{-1}). The heavy chain dashed lines represent the observed measurements, the heavy dotted lines represent the simulated discharge for the present by the WEM, the solid lines represent the simulated discharge in the future, and the thin dotted lines represent the present simulations for the individual model.

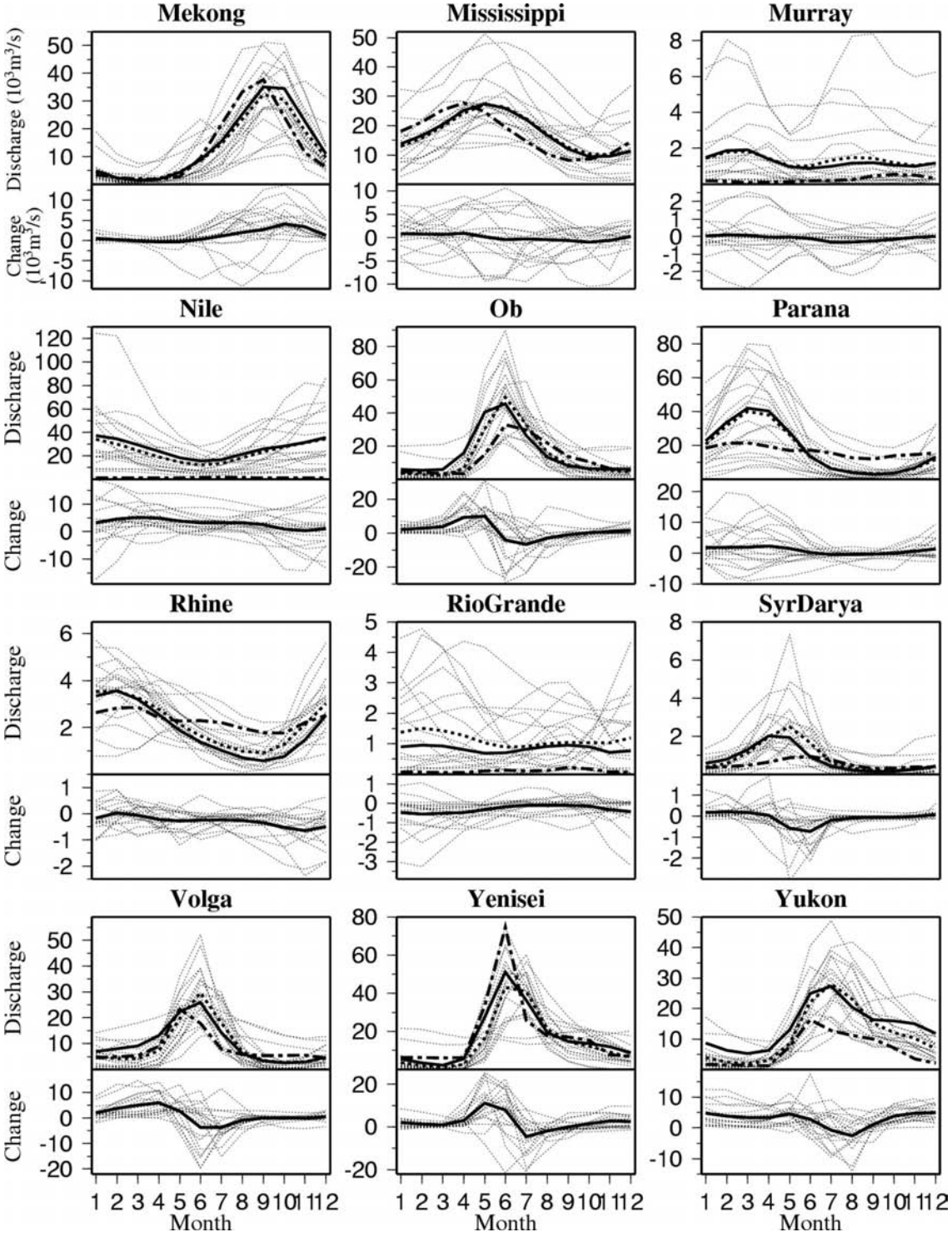

FIG. 9. (*Continued*)

January to July, the discharge increases in the future. However, these trends may be statistically insignificant, considering the range of uncertainty due to smaller normalized runoff change in Fig. 6.

It is difficult to reproduce the discharge from rivers in arid areas (Amu Darya, Euphrates, Huang He, Murray, Nile, Rio Grande, and Syr Darya) because of the sensitivity to water usage by irrigation and dams, as well as

TABLE 4. Annual mean discharge of observation, present simulation, and future. The asterisk (*) denotes that the absolute value of normalized discharge change exceeds 1.

River basin	Observation ($m^3 s^{-1}$)	Present ($m^3 s^{-1}$)	RRMS (%)	Future ($m^3 s^{-1}$)	Change (%)
Amazon	172 871.	90 353.	50.1	95 255.	5.4
Amu Darya	1492.	2048.	98.6	2039.	−0.4
Amur	10 083.	10 525.	19.1	12 150.	15.4
Changjiang	28 171.	34 955.	32.7	37 674.	7.8
Columbia	5178.	8770.	111.9	9334.	6.4
Congo	40 250.	65 174.	77.7	68 045.	4.4
Danube	6415.	6142.	28.6	4799.	−21.9*
Euphrates	522.	608.	80.2	376.	−38.1
Ganges	12 294.	9009.	58.7	10 635.	18.0
Huang He	1423.	8172.	544.6	9214.	12.8
Lena	15 155.	13 136.	93.6	16 283.	24.0*
MacKenzie	9025.	12 275.	62.6	14 271.	16.3
Mekong	13 061.	12 746.	38.1	14 009.	9.9
Mississippi	16 952.	17 488.	29.2	17 527.	0.2
Murray	259.	1345.	442.1	1254.	−6.8
Nile	1251.	23 549.	1886.7	26 530.	12.7
Ob	12 617.	14 078.	56.8	15 505.	10.1
Parana	16 595.	17 142.	63.2	17 989.	4.9
Rhine	2315.	2207.	28.3	1914.	−13.3
Rio Grande	106.	1145.	1001.4	839.	−26.7
Syr Darya	517.	846.	131.5	759.	−10.3
Volga	8300.	9033.	58.4	9968.	10.4
Yenisei	18 563.	14 459.	62.3	16 709.	15.6
Yukon	6379.	11 462.	104.9	14 284.	24.6

evaporation from the river surface. WEM projects decreasing trends of the annual mean discharge from the Euphrates (−38.1%), Syr Darya (−10.3%), and Rio Grande River (−26.7%). In particular, discharges from the Euphrates and Syr Darya clearly decrease during the high-water season. In contrast, the annual means of the discharge from the Huang He and the Nile increase by +12.8% and +12.7% due to increase in runoff in watershed regions.

The reproduced discharges in the midlatitude rainy area (Columbia, Danube, Mississippi, Parana, Rhine, and Volga) represent the seasonal cycle similar to those obtained by the observation, but the peak timing shifts about one month earlier or later. Nevertheless, the discharges from the Parana and Rhine do not match those obtained by observation because the Parana and Rhine are highly regulated by reservoirs. The discharges from the Danube and Rhine decrease in the future (−21.9% and −13.3%) because of the decrease in precipitation over the Mediterranean region to the Caspian Sea region as indicated in Figs. 3 and 6. The peak timing in the Columbia River basin shifts about three months earlier due to earlier onset of snowmelt in the Rocky Mountain areas. The future discharge from the Mississippi is similar to that at the present. In the Volga, the discharge increases during the low-water season, but it decreases during the high-water season. The annual mean discharge then results in an increasing trend (+10.4%).

The discharge from the rivers in the Asian monsoon region (Changjiang, Ganges, and Mekong) is sensitive to the seasonal cycle in precipitation. The magnitude and timing of the simulated discharge nearly correspond with those obtained by observations. The amounts of the discharge from the Changjiang, Ganges, and Mekong increase (+7.8%, +18.0%, and +9.9%) in the future. However, those trends may be statistically insignificant, considering the range of uncertainty due to smaller normalized runoff change (Fig. 6).

In high latitudes (Amur, Lena, MacKenzie, Ob, Yenisei, and Yukon), the magnitude and seasonal cycle of the simulated discharges correspond well to those obtained by the observations except for the peak magnitude. The changes in the discharge clearly increase by +15.4%, +24.0%, +16.3%, +10.1%, +15.6%, and +24.6%, due to significant increase in the precipitation (Fig. 3). The average discharge from the four rivers (Lena, MacKenzie, Ob, and Yenisei) into the Arctic Ocean increases by about 16%, which is a smaller increase than estimated by Peterson et al. (2002) and Arnell (2005). Additionally, the peak timings of the discharges occur earlier because the snowmelting season becomes earlier as a result of global warming.

5. Summary and discussion

This study investigated the projections of the river discharge from 24 rivers during the twenty-first century simulated by 19 AOGCM simulations based on the SRES A1B scenario. The river discharge is estimated by the river flow model (GRiveT), which transports the runoff water along the river routing. To reduce model biases and uncertainties for the projection, a weighted ensemble mean (WEM) is utilized to estimate the river discharge in the present as well as in the future. The WEM performance of the reproduced climatology for the present precipitation is found to be superior to that of the simple ensemble mean. Although it is difficult to reproduce present river discharges in an individual model, the results of the WEM of the discharges can make a more accurate reproduction for most rivers, except those affected by water usage (e.g., irrigation and dams) and evaporation from the river surface.

Our results suggest that the annual mean precipitation, evaporation, and runoff in the future increase in high latitudes of the Northern Hemisphere, southern to eastern Asia, and central Africa. In contrast, they decrease in the Mediterranean region, southern Africa, southern North America, and Central America. The change ratio of the global mean runoff is larger than the precipitation change. Nevertheless, the area where reliable runoff change is projected is smaller than that of the changes in precipitation and evaporation. Although the spatial distribution of the changes in the precipitation and runoff tends to coincide with that in the river discharge, it should be emphasized that the change of runoff in the upstream region affects the river flow in the downstream region. In the high-latitude rivers (Amur, Lena, MacKenzie, Ob, Yenisei, and Yukon), the discharges increase, and the peak timings shift earlier due to the earlier snowmelt caused by global warming. This study indicates that the average discharge into the Arctic Ocean increases by 16%, which is smaller than previous estimates by Peterson et al. (2002) and Arnell (2005). In the rivers in Europe to the Mediterranean (Danube, Euphrates, and Rhine), and southern North America (Rio Grande), the discharges tend to decrease.

The simulated surface water that occurs as a result of precipitation is allocated to runoff and evaporation. The difference in the allocation to runoff and evaporation is attributed to the characteristics of the climatology (Budyko 1974). In rainy or wetland areas (e.g., the Tropics), an increment of precipitation is primarily allocated to runoff rather than to evaporation, because the amount of evaporation is nearly constant due to the already saturated land surface condition. Therefore, in southern to southeastern Asia and the Amazon, the increase of runoff is larger than that of evaporation when precipitation is increasing. Additionally, in the Arctic tundra, the increase in runoff is also larger than the increase in evaporation because the surface of tundra is always wet. On the other hand, since the increment in precipitation in the arid area is mostly allocated to evaporation, the decrease in runoff is larger than that in evaporation when precipitation is decreasing in regions such as Europe, the Mediterranean, and central Eurasia.

It is widely accepted that the projection of the river discharges is useful for a risk assessment of the water resources. However, it is necessary to consider the changes in water resources by human activities (Oki et al. 2003) and to consider extreme weather and climate events such as floods and drought (Milly et al. 2002). Since the variability of the changes in discharge is larger than that in precipitation and evaporation, it is generally difficult to project river discharges. Therefore, it is necessary to improve the land surface scheme in AOGCM and also to develop appropriate multimodel analysis methodology for the projections of river discharge.

Acknowledgments. We acknowledge the international modeling groups for providing their data for analysis, the Program for Climate Model Diagnosis and Intercomparison (PCMDI) for collecting and archiving the model data, the JSC/CLIVAR Working Group on Coupled Modelling (WGCM) and their Coupled Model Intercomparison Project (CMIP) and Climate Simulation Panel for organizing the model data analysis activity, and the IPCC WG1 TSU for technical support. The IPCC Data Archive at Lawrence Livermore National Laboratory is supported by the Office of Science, U.S. Department of Energy. The authors thank Global Runoff Data Centre for providing river discharge datasets. The authors wish to thank anonymous referees and Drs. K. Sunada, H. L. Tanaka, T. Nakaegawa, M. E. Hori, and O. Arakawa for their valuable comments and helpful advice.

REFERENCES

Adler, R. F., and Coauthors, 2003: The version-2 Global Precipitation Climatology Project (GPCP) monthly precipitation analysis (1979–present). *J. Hydrometeor.,* **4,** 1147–1167.

Arnell, N. W., 1999: Climate change and global water resources. *Global Environ. Change,* **9,** S31–S49.

——, 2004: Climate change and global water resources: SRES emissions and socio-economic scenarios. *Global Environ. Change,* **14,** 31–52.

——, 2005: Implications of climate change for freshwater inflows to the Arctic Ocean. *J. Geophys. Res.,* **110,** D07105, doi:10.1029/2004JD005348.

——, M. J. L. Livermore, S. Kovats, P. E. Levy, R. Nicholls, M. L. Parry, and S. R. Gaffin, 2004: Climate and socio-economic scenarios for global-scale climate change impacts assessments: Characterising the SRES storylines. *Global Environ. Change,* **14,** 3–20.

Arora, V. K., and G. J. Boer, 1999: A variable velocity flow routing algorithm for GCMs. *J. Geophys. Res.,* **104** (D24), 30 965–30 979.

——, and ——, 2001: Effects of simulated climate change on the hydrology of major river basins. *J. Geophys. Res.,* **106** (D4), 3335–3348.

Budyko, M. I., 1974: *Climate and Life.* Academic Press, 510 pp.

Fritsch, J. M., J. Hilliker, J. Ross, and R. L. Vislocky, 2000: Model consensus. *Wea. Forecasting,* **15,** 571–582.

Giorgi, F., and L. O. Mearns, 2002: Calculation of average, uncertainty range, and reliability of regional climate changes from AOGCM simulations via the "Reliability Ensemble Average" (REA) method. *J. Climate,* **15,** 1141–1158.

Harrison, M. S. J., T. N. Palmer, D. S. Richardson, and R. Buizza, 1999: Analysis and model dependencies in medium-range ensembles: Two transplant case-studies. *Quart. J. Roy. Meteor. Soc.,* **125,** 2487–2515.

Houghton, J. T., Y. Ding, D. J. Griggs, M. Noguer, P. J. van der Linden, and D. Xiaosu, Eds., 2001: *Climate Change 2001: The Scientific Basis.* Cambridge University Press, 944 pp.

Krishnamurti, T. N., C. M. Kishtawal, T. E. LaRow, D. R. Bachiochi, Z. Zhanf, C. E. Willifor, S. Gadgil, and S. Surendran, 1999: Improved weather and seasonal climate forecasts from multimodel superensemble. *Science,* **285,** 1548–1550.

Manabe, S., P. C. D. Milly, and R. Wetherald, 2004: Simulated long-term changes in river discharge and soil moisture due to global warming. *Hydrol. Sci. Bull.,* **49,** 625–642.

McCarthy, J. M., O. F. Canziani, N. A. Leary, D. J. Dokken, and K. S. White, Eds., 2001: *Climate Change 2001: Impacts, Adaptation, and Vulnerability.* Cambridge University Press, 1000 pp.

Meehl, G. A., C. Covey, B. McAvaney, M. Latif, and R. J. Stouffer, 2005: Overview of the coupled model intercomparison project. *Bull. Amer. Meteor. Soc.,* **86,** 89–93.

Milly, P. C. D., R. T. Wetherald, K. A. Dunne, and T. L. Delworth, 2002: Increasing risk of great floods in a changing climate. *Nature,* **415,** 514–517.

Min, S.-K., E.-H. Park, and W.-T. Kwon, 2004: Future projection of East Asian climate change from multi-AOGCM ensemble of IPCC SRES scenario simulations. *J. Meteor. Soc. Japan,* **82,** 1187–1211.

Nakicenovic, N., and R. Swart, Eds., 2000: *Emissions Scenarios*. Cambridge University Press, 570 pp.

Nijssen, B., G. M. O'Donnell, D. P. Lettenmaier, D. Lohmann, and E. F. Wood, 2001: Predicting the discharge of global rivers. *J. Climate,* **14,** 3307–3323.

Oki, T., and Y. C. Sud, 1998: Design of Total Runoff Integrating Pathways (TRIP)—A global river channel network. *Earth Interactions,* **2.** [Available online at http://EarthInteractions.org.]

——, T. Nishimura, and P. Dirmeyer, 1999: Assessment of annual runoff from land surface models using Total Runoff Integrating Pathways (TRIP). *J. Meteor. Soc. Japan,* **77,** 235–255.

——, Y. Agata, S. Kanae, T. Saruhashi, and K. Musiake, 2003: Global water resources assessment under climatic change in 2050 using TRIP. *IAHS Publ.,* **280,** 124–133.

Palmer, T. N., Č. Branković, and D. S. Richardson, 2000: A probability and decision-model analysis of PROVOST seasonal multi-model ensemble integration. *Quart. J. Roy. Meteor. Soc.,* **126,** 2012–2033.

Peterson, B. J., R. M. Holmes, J. W. McClelland, C. J. Vörösmarty, R. B. Lammers, A. I. Shiklomanov, I. A. Shiklomanov, and S. Rahmstorf, 2002: Increasing river discharge to the Arctic Ocean. *Science,* **298,** 2171–2173.

Seckler, D., R. Barker, and U. Amarasinghe, 1999: Water scarcity in the twenty-first century. *Water Resour. Dev.,* **15,** 29–42.

Vörösmarty, C. J., P. Green, J. Salisbury, and R. B. Lammers, 2000: Global water resources: Vulnerability from climate change and population growth. *Science,* **289,** 284–288.

Wu, P., R. Wood, and P. Stott, 2005: Human influence on increasing Arctic river discharges. *Geophys. Res. Lett.,* **32,** L02703, doi:10.1029/2004GL021570.